Effects of the Equivalent Geometric Nodal Imperfections on the stability of single layer grid shells

Effects of the Equivalent Geometric Nodal Imperfections on the Stability of Single Layer Grid Shells

Luca Bruno[a,*], Mario Sassone[a], Fiammetta Venuti[b]

[a] *Politecnico di Torino, Department of Architecture and Design, Viale Mattioli 39, I-10125, Torino, Italy*
[b] *Politecnico di Torino, Department of Structural and Geotechnical Engineering, Corso Duca degli Abruzzi 24, I-10129, Torino, Italy*

Abstract

The present paper discusses the sensitivity of the global and local stability of a hybrid single layer grid shell to a set of equivalent geometric nodal imperfections representative of the actual structural and construction imperfections. Since imperfections are hard to be measured and controlled in experimental facilities, the stability of the structure is extensively investigated in numerical experiments. The imperfections are set by means of the so-called Eigenmode Imperfection Method. The method parameter space is densely sampled, and different structural models are adopted. The results are given in terms of two bulk parameters: the well established Load Factor and the proposed Buckling Shape Length, the latter being introduced to provide a continuous measure of the degree of "globalness" of the instability. Significant and non monotonic changes in both the Load Factor and Buckling Shape Length are observed versus the growth of the imperfection amplitude. Further, a local metrics of the grid shell geometry, named nodal apex, is introduced for each structural node. Special emphasis is given to the analysis of the correlation between the apex of the initial imperfect geometry and the apex of the deformed shape at collapse. The observed high correlation suggests that the mechanical behaviour of the imperfect grid shell is significantly influenced by this local geometrical feature.

Keywords: single layer grid shell, buckling instability, equivalent geometric nodal imperfection, Eigenmode Imperfection Method

Nomenclature

BSL	Buckling Shape Length
CIMM	Consistent Imperfection Mode Method
EGNI	Equivalent Geometric Nodal Imperfection
EIM	Eigenmode Imperfection Method
GMNA (GMNIA)	Geometrically and Materially Nonlinear Analysis of the perfect (imperfect) structure
GNA (GNIA)	Geometrically Nonlinear Analysis of the perfect (imperfect) structure
LBA (LBIA)	Linear Buckling Analysis of the perfect (imperfect) structure
LF	Load Factor
LC-NR	Load Control by Newton Raphson
AL-NR	Arc-Length by Newton Raphson
SLGS	Single Layer Grid Shell
USL	Ultimate Limit State
L	dome span length
f	dome rise length

*Corresponding author. Tel: (+39) 011-090.4870
Email address: luca.bruno@polito.it (Luca Bruno)

l	characteristic length of quadrangular fields
p	subscript of the generic structural node
P	number of structural nodes
x	horizontal space coordinate
y	horizontal space coordinate
z	vertical space coordinate
K	nodal apex
$\mathbf{K}_e$	elastic stiffness matrix
$\mathbf{K}_g$	geometric stiffness matrix
k	weighting factor
Q	nodal resultant load
q	uniform load
s	uniform live (snow) load
g	dead load
A	quadrangular field surface
f_y	yield strength
R	correlation coefficient
α	imperfection amplitude
α^*	dimensionless imperfection amplitude
ν	nodal direction
μ	load multiplier
σ_0	cable initial prestressing
σ	stress field
η	equivalent nodal imperfection field
ϕ	buckling mode shape
φ	generic buckling shape
λ	eigenvalue
δ	nodal displacement
δ^u	ultimate nodal deflection
κ	cotangent of the nodal angle
0	superscript for the perfect geometry

1. Introduction

Buckling instability is the Ultimate Limit State (ULS) that drives the design of Single Layer Grid Shells (SLGS) [1]. The SLGS buckling instability has been early recognized to be highly sensitive to imperfections [1]. Codes and Standards (e.g. [2],[3]) actually recommend to take into account the effects of imperfections in the structural design of grid shells. Imperfections can be ascribed to imperfect constraints, single member mechanical imperfections, loading imperfections, or geometrical ones. In particular, geometrical imperfections can be induced by single member curvature or nodal imperfections, e.g. the ones due to factory defects or assembly tolerances. Generally speaking, the geometrical imperfections result in a nodal deviation from design. To the authors' best knowledge, a statistical characterization of these nodal deviations as a field of nodal random variables is not available in the literature for SLGS, while detailed measurements and related statistics have been recently proposed for continuous shells (e.g. [4]). Hence, a so-called Equivalent Geometric Nodal Imperfection (EGNI) is usually adopted in the design practice of SLGS. In a worst case scenario perspective, EGNI is assumed to be a deterministic, semi-empirical imperfection field aimed at inducing the lowest load factor. In some early studies, e.g. [5], the worst shapes of imperfections for simple space trusses have been obtained in closed form solution. At the same time, others studies, e.g. [6], initiated the search of the worst case imperfection field by means of numerical experiments.

Different methods are currently available to assign the design EGNI. Some authors [7, 8] classify these methods into three categories: i. the so-called random imperfection mode method, ii. the Consistent Imperfection Mode

Method (CIMM) and iii. the Eigenmode Imperfection Method (EIM). According to both CIMM and EIM, the imperfection field is described in term of a deterministic spatial distribution normalized to unit (or imperfection shape, in literature) and of an imperfection amplitude. The EIM is the most popular one in the design practice. It is critically reviewed, applied and discussed in the present study.

The normalized *spatial distribution* is assumed to be equal to one of the buckling eigenmodes of the perfect structure evaluated by a Linear Buckling Analysis (LBA). The first eigenmode corresponds to the lowest eigenvalue, i.e to the lowest load multiplier. For this reason, it is conjectured to be representative of the most critical imperfection shape, at least at the initial stage of the buckling. Using the first eigenmode is common design practice, and has been used for instance in the design of existing grid shells, e.g. [9, 10]. Nevertheless, some researchers [11, 12, 13] have obtained lower failure loads adopting higher mode shapes as the imperfection. The EIM can be extended by shaping the imperfection according to a linear combination of two or several mode shapes. According to Bulenda and Knippers [14], "there are apparently no rules on how to combine the eigenmodes to find the decisive imperfection. Thus the engineer has to go the long way of computing the failure loads for different combinations of eigenmodes to develop a feeling for the imperfection sensitivity of the structure and for the choice of the proper imperfection".

The *imperfection amplitude* is usually defined as the maximum deviation from the perfect geometry along the direction normal to a reference surface. It is usually scaled with respect to the SLGS span length L, even if some authors, e.g. [15], normalize it by the equivalent shell thickness. A huge variability of the imperfection amplitude can be recognized in the design practice. Let us provide some examples: in their seminal work, Bulenda and Knippers [14] provide $L/500$ as an example of reasonable value; more recently, an imperfection of 3 mm has been chosen in [16], looking at the tolerance used in the construction of two steel grid shells, the Schubert Band [17] and the Great Court at the British Museum [9]. Bearing in mind that a spherical cap with $L = 30.5$ m is adopted in [16], a very small imperfection amplitude of about $L/10000$ follows. Face to such a variability, a number of recent parametrical studies [14, 8, 13, 15, 18, 7] have investigated the sensitivity of the SLGS instability to the EGNI amplitude. In the cited studies, the sensitivity of the Load Factor (LF), i.e. the load multiplier at the critical point, is quantitatively evaluated, while the corresponding deflection field is discussed in qualitative terms only. A non exhaustive collection of the results available in literature is provided in Figure 1, where the Load Factor LF/LF^0 is plotted versus the scaled imperfection amplitude α/L, being LF^0 the load factor of the perfect SLGS, i.e. at $\alpha = 0$. The studied synclastic SLGS

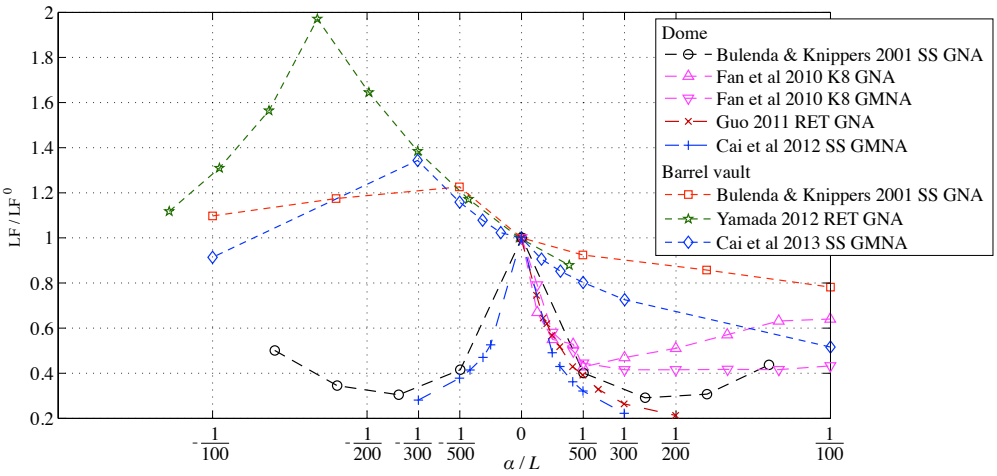

Figure 1: Scaled Load Factor (LF/LF^0) versus the scaled imperfection amplitude α/L: studies in literature

are first categorized in two types according to the geometry of the reference surface, i.e. domes with double curvature and barrel vaults with single curvature. A further categorization refers to the truss arrangement: Schlaich and Schober (SS, [19]) hybrid SLGS having quadrangular fields diagonally braced by prestressed cables, and Kiewitt-8 (K8) or reticulated (RET) grid shells having triangular fields. The reviewed studies adopt Geometrically Nonlinear Analysis (GNA) and/or Geometrically and Materially Nonlinear Analysis (GMNA) to evaluate the effect of the imperfection

on the buckling instability. It is worth pointing out that, in the cited studies, the amplitude is assumed to be signed. Domes are by far less sensitive than barrel vaults to the sign of the amplitude. The LF for barrel vaults shows a monotonic decreasing trend for positive amplitudes. The LF for domes abruptly decreases for small amplitudes, but its trend versus α is no longer monotonically decreasing at least for two setups when GNA is adopted and medium to large amplitudes (e.g. $\alpha \geq 1/500$) are considered. Face to this general trend, local minima or maxima cannot be a priori excluded because the considered range of imperfection amplitude is not densely sampled.

To the authors' best knowledge, the EIM is currently codified in two standards, i.e. the Eurocode 3: Design of steel structures - Part 1-6: Strength and stability of shell structures [3] and the Technical specification for reticulated shells JGJ61-2003 [2]. While in [2] the fundamental mode shape is prescribed, in [3] the "eigenmode-affine pattern", i.e. the buckling mode shape associated to the lowest eigenvalue, should be used as the imperfection shape "unless a different unfavourable pattern can be justified". In particular, [3] echoes Bulenda and Knippers: "If the most unfavorable pattern cannot be readily identified beyond reasonable doubt, the analysis should be carried out for a sufficient number of different imperfection patterns, and the worst case should be identified." The imperfection amplitude for SLGS is explicitly codified only in [2]: the maximum geometric imperfection that is caused by construction should be restricted within $L/300$. Finally, both codes allow to adopt different kind of structural analysis with increasing expected accuracy, i.e. LBA, GNA, GMNA, to evaluate the effects of the EGNI on the buckling stability.

According to the writers, some questions immediately follow the state of the art shortly reviewed above. Does the conjectured rule "the higher the imperfection, the lower the load factor" always hold? Or, in other terms, do local maxima or minima exist in the trend of the LF versus the imperfection amplitude? Does such a trend reflect a change in the buckling shape at collapse? And does the imperfection amplitude also involve a switch from global to local instabilities? Does a value of the imperfection amplitude exist below which the buckling stability is not affected by the imperfections? In which way the choice and combination of the buckling mode shapes affect the buckling stability? In which way the different methods of structural analysis propagate the effects of the EIM-based imperfections on the buckling stability? Finally, does a general connection based on a sound mechanical reading can be recognized between the adopted EGNI field and the simulated Buckling Limit State?

The present study aims at shedding some light on such issues. In particular: i. the EIM is critically discussed by densely sampling its free parameters, i.e. the imperfection amplitude and its spatial distribution. The effects on the buckling ULS are scrutinized, in terms of both load factor and deformed shape of the SLGS; ii. the sensitivity of different structural models (LBA, GNA, GMNA) to the EIM parameters is investigated; iii. the EGNI amplitude and its spatial distribution are correlated with the mechanical response of the grid shell, and with its deflection at collapse in particular.

In Section 2 the modelling and computational approach are briefly recalled. The structural setup selected for the application is described in Section 3 together with the parametric analysis plan and the bulk parameters selected for post processing. The results of the sensitivity analysis are provided in Section 4.3, while a mechanical insight on the results is proposed in Section 4.4. Finally, conclusions and perspectives are outlined in Section 5.

2. Modelling approach

2.1. Structural modelling

Three structural models of increasing complexity and accuracy are considered and briefly recalled in the following in their discrete form:

Linear Buckling Analysis (LBA) The linear buckling analysis solves the eigenvalue problem

$$\left[\mathbf{K}_e + \lambda \mathbf{K}_g\left(\sigma\right)\right]\mathbf{\Phi} = 0, \tag{1}$$

where $\boldsymbol{\lambda}$ is the vector of load factors and $\mathbf{\Phi}$ is the matrix of the associated buckling mode shapes. The geometric stiffness $\mathbf{K}_g\left(\sigma\right)$ is a function of the stress field σ. $\mathbf{K}_g$ is evaluated through a static analysis that solves the equation

$$\left[\mathbf{K}_e + \mathbf{K}_g\left(\sigma_0\right)\right]\delta = \mathbf{Q} \tag{2}$$

where $\mathbf{K}_e$ is the elastic stiffness, $\mathbf{K}_g\left(\sigma_0\right)$ accounts for the initial prestress σ_0, if any, and $\mathbf{Q}$ is the applied load.

Geometrically Nonlinear elastic Analysis (GNA)

$$\left[\mathbf{K}_e + \mathbf{K}_g(\boldsymbol{\delta})\right]\boldsymbol{\delta} = \mu\mathbf{Q} \tag{3}$$

where the geometric stiffness $\mathbf{K}_g(\boldsymbol{\delta})$ is a function of the displacement field $\boldsymbol{\delta}(\sigma)$ and μ is the load multiplier that increases along the simulation.

Geometrically and Materially Nonlinear Analysis (GMNA)

$$\left[\mathbf{K}_e(\boldsymbol{\delta}) + \mathbf{K}_g(\boldsymbol{\delta})\right]\boldsymbol{\delta} = \mu\mathbf{Q} \tag{4}$$

In the study, the steel nonlinear stress-strain relation is modelled by a bilinear law (elastic-perfect plastic). Due to the progressive yielding of members under monotonically increasing load, the overall structural behaviour is described by a tangent stiffness matrix $\mathbf{K}_e$ which softens for increasing displacement field $\boldsymbol{\delta}(\sigma)$.

In the following, when applied to the imperfect geometry, the above structural models are named LBIA, GNIA and GMNIA, according to [3].
The structural analysis is performed by means of the finite-element code ANSYS ©v14.0. The Load Control (LC-NR) and the Arc-Length (AL-NR) path-following procedures are applied, where the iterative convergence is accomplished in both cases at each step by means of the standard Newton Raphson (NR) method [20].
The computations are carried out on a single Intel i7-4702MQ, 2.20 GHz CPU with 8 GB of RAM memory.

2.2. Definition of the observables

Besides local observables in space, two bulk parameters are adopted in order to provide a synthetic description of the mechanical behaviour of the grid shell versus the nodal imperfections. They are defined in the following with reference to a grid shell with P structural nodes having coordinates $\mathbf{X}(p) = \left\{x_p, y_p, z_p\right\}$ $(p = 1, P)$.

Load Factor (LF). The load factor is the most relevant parameter usually considered in Buckling Limit State. Its definition is herein recalled:

$$\mathbf{Q}^u = LF\ \mathbf{Q} \tag{5}$$

where $\mathbf{Q}^u$ is the ultimate buckling load and $\mathbf{Q}$ is the load condition as defined in Section 3. Within LBA, the Load Factor is equal to $LF = \lambda^1$, i.e. the lowest eigenvalue, which corresponds to the buckling mode shape $\boldsymbol{\phi}^u$. Within both GNA and GMNA, the Load Factor is equal to $LF = \mu^u$, being μ^u the load multiplier that induces the collapse ($dQ/d\delta = 0$ in a selected reference node), i.e. reaching a limit point, and $\boldsymbol{\delta}^u$ the corresponding displacement field.

Buckling Shape Length (BSL). Usually grid shell instability is categorized according to the amount of nodes or structural members involved in the collapse. Besides the single-member buckling [21], "local" or "global" instabilities can occur, where the former involves the snap-through of a single node or of the surrounding ones, while in the latter the structure buckles as a whole. More precisely a global collapse is the one having large nodal displacements almost uniformly spread along the whole structure. Conversely, a local collapse is the one having large nodal displacements clustered in limited regions. Furthermore, a combination of the above can occur, because SLGS optimization tends to produce a condition in which local and global collapses are close to each other [5, 1]. In order to provide a quantitative, continuous measure of the degree of "globalness" of the instability, or conversely of its "localness", a new observable, called Buckling Shape Length, is proposed. The BSL is defined here as

$$BSL = \frac{3}{P^2 L}\sum_{i=1}^{P}\sum_{j=1}^{P}\left[\sqrt{\left(x_i - x_j\right)^2 + \left(y_i - y_j\right)^2 + \left(z_i - z_j\right)^2}\frac{|\varphi_j|}{|\hat{\varphi}|}\right], \tag{6}$$

where subscripts i and j refer to two generic nodes, x, y and z are their coordinates, φ_j is the value in the j-th node of the generic buckling shape $\boldsymbol{\varphi}$ and $|\hat{\varphi}|$ is the maximum value of the latter. $\boldsymbol{\varphi}$ can be the buckling mode

shape $\boldsymbol{\phi}^u$ or the structural deflection at collapse $\boldsymbol{\delta}^u$, depending on the adopted structural model. According to Eq. (6), the BSL is bounded within the range [0 1].

The higher the BSL, the higher the degree of globalness of the collapse mechanism, in the sense that the deflection shows high values at spaced structural nodes. For the sake of clarity, the BSL is applied to some synthetic 1D deflection fields $\varphi(x)$ in the following, and the results are shown in Figure 2. In particular, in

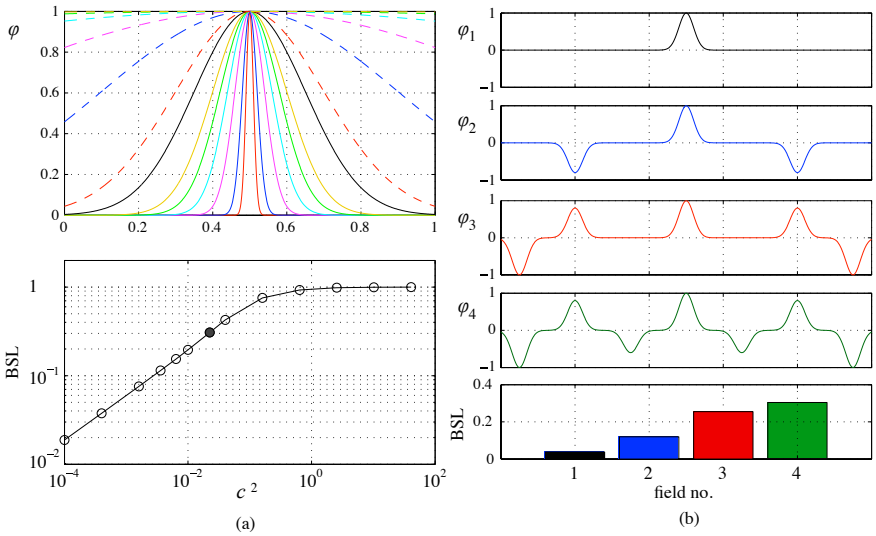

Figure 2: Buckling Shape Length evaluated for test case 1D fields: gaussian field (a), multi maxima field (b)

Figure 2-a the field is analytically expressed by the normalized gaussian function $\varphi(x) = \exp -\frac{(x-b)^2}{2c^2}$ having constant localization parameter $b = 0.5x/L$ and increasing size parameter $1e-2 \leq c \leq 6.5$. The larger the bell width, the higher the BSL value, and $\lim_{c\to 0} BSL = 0$, $\lim_{c\to\infty} BSL = 1$. In particular, if most of the bell is within the x range ($c \leq 0.15$, black line and point), the BSL linearly depends on c^2. The synthetic fields φ_i in Figure 2-b mimic in 1D the typical buckling mode shapes of SLGS domes (see e.g. Fig. 8-3a for the perfect setup adopted in this study). They are characterized by multiple local maxima (or minima) and are arranged for increasing degree of globalness. Once more, BSL shows its ability to provide a measure of such a globalness. Once the BSL for the perfect structure is defined, the effects of the EGNI on the degree of globalness of the collapse mechanism can be quantitatively assessed.

3. Benchmark description

The choice of the geometrical and structural setups of the perfect SLGS to be adopted as benchmark aims at obtaining a form-resistant and slender structure, for which the buckling instability in the elastic regime is expected to prevail on the yielding failure. The perfect geometry in relation to the load condition, the structural element cross section, the internal joints are all chosen for this purpose. A Schlaich and Schober [19] hybrid SLGS is selected as a suitable reference to build the benchmark setup coherently with the aims above.

3.1. Geometrical setup

The perfect geometry of the investigated single-layer grid shell is shown in Figure 3. The analytical form of the reference continuous dome (Fig. 3-a) belongs to the translational surface type, having a parabola as both the directrix and generatrix, i.e. it is a paraboloid. Its main geometrical parameters are: span length $L = 30$ m, span to rise ratio $L/f = 8$ (Fig. 3-d).

The perfect discrete grid shell geometry results from the point wise sampling of the dome surface in P structural nodes ($p = 1, P$) along the directions of the directrix and generatrix having coordinates $\mathbf{X}^0(p) = \left\{x_p^0, y_p^0, z_p^0\right\}$, where the

superscript 0 refers to the perfect setup. The nodal coordinates are rounded to 6 decimal places in order to describe the perfect geometry with a precision higher than the considered lowest imperfection amplitude ($\alpha = 1e-5$ m, see Sect. 3.3). The nodes are connected along the directions of the directrix and generatrix by straight segments resulting in elemental planar quadrangular fields [22], having a characteristic length $l \approx 1.5$ m (Fig. 3-b). Each quadrangular field is braced by two diagonal cables, as shown in Figure 3-c.

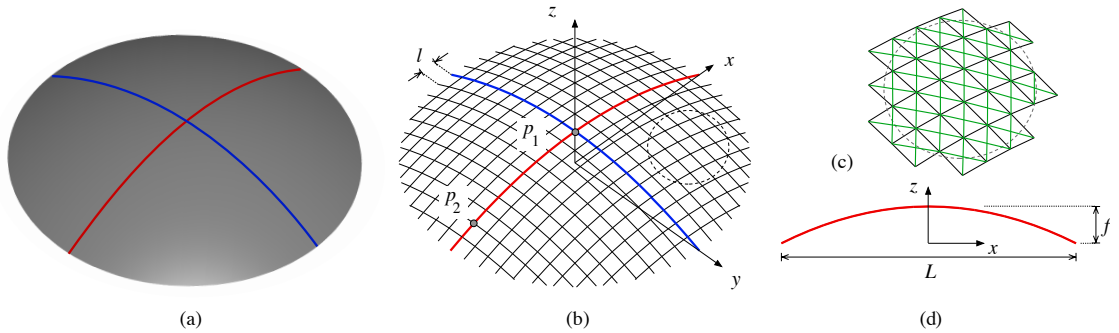

Figure 3: Setup geometry: reference continuous shell surface (a), discrete grid shell surface (b, shown without cables), close-up view of a part of the dome including diagonal cables (c), section along the meridian vertical plane (d)

The mechanical performances of both continuous shells and grid shells, including their stability, are mainly driven by their geometry. While the geometry of continuous dome shells is described by well-defined quantities, their application to discrete grid shells is not straightforward. The angle between members located along the meridian lines has been defined by [23] for single-layer spherical domes having triangular grid arranged along meridians and rings. This angle mimics the meridian simple curvature of the corresponding reference surface. It is recognized to be highly influential on the grid shell buckling instability. In the following, a preliminary attempt is paid to define nodal quantities analogous to the gaussian curvature and the surface normal unit vector. The definition holds for any kind of shell geometry and for grids having four members connected in each node. The nodal apex $K(p)$ [m^{-2}] (Figure 4) mimics at each node p the gaussian curvature in the continuous analogy. The nodal direction $\nu(p)$ mimics at each node the normal unit vector. With reference to Figure 4-a, which represents the p-th node and its four adjacent nodes, the nodal apex $K(p)$ is defined as follows:

$$K(p) = \kappa_1 \kappa_2, \tag{7}$$

where $\kappa_1 = \cot(\mathcal{W}\widehat{p}\mathcal{E}/2)$ and $\kappa_2 = \cot(\mathcal{S}\widehat{p}\mathcal{N}/2)$ (Fig. 4-b). The choice of the cotangent function assures the value of K is in the range $[0\ \infty]$. In particular, $K = 0$ if one of the angles above is equal to π, while $K = \infty$ if one of the angles is equal to 0. As for the nodal direction, the unit vector $\nu(p)$ is determined from the intersection of two planes λ and β (Fig. 4-c), respectively normal to the planes $(\mathcal{W}p\mathcal{E})$ and $(\mathcal{S}p\mathcal{N})$. The positive direction of $\nu(p)$ is upward and follows from counterclockwise ordering of the adjacent nodes, i.e. $\mathcal{E}$-$\mathcal{N}$-$\mathcal{W}$-$\mathcal{S}$. The signs of κ_1 and κ_2 is determined through projection of the $(\mathcal{W}\widehat{p}\mathcal{E})$ and $(\mathcal{S}\widehat{p}\mathcal{N})$ bisectors on $\nu(p)$. In Figure 5, the gaussian curvature of the reference continuous shell surface and the nodal apex of the discrete grid shell are compared showing a perfect equivalence.

3.2. Structural setup

The grid of quadrangles is formed by steel beams. These are diagonally braced by prestressed cables. The structures are covered with glass. The glass panels do not have structural function but have to be intended as dead load only.

The main properties of the structural elements are given in Table 1, together with the corresponding Finite Element adopted in the ANSYS©code. The beam cross section mimics the ones usually used by [19, 14], i.e. a solid rectangular cross section. The 3D beam elements are based on Timoshenko beam theory and adopts a cubic shape function. The cables are modelled by 3D tension-only trusses within non linear analysis.

The whole structure is assumed to be hinged at the boundaries, while the joints between steel bars are modelled as rigid, as usually done in the literature [14, 18, 8]. In fact, the joint type is expected to lightly affect the buckling

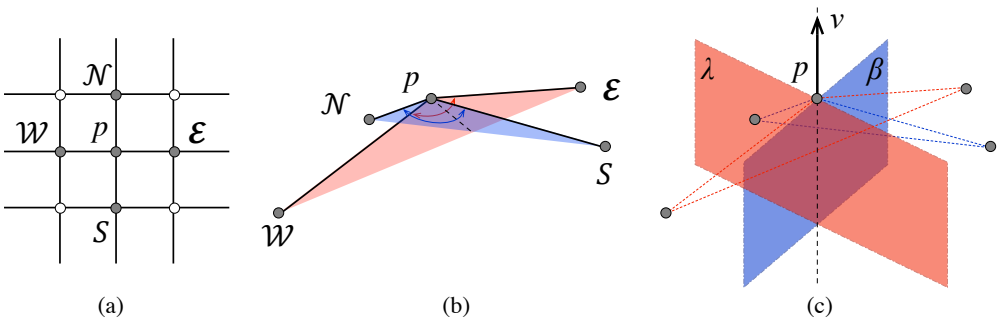

Figure 4: Definition of the nodal direction $v(p)$ and the nodal apex $K(p)$

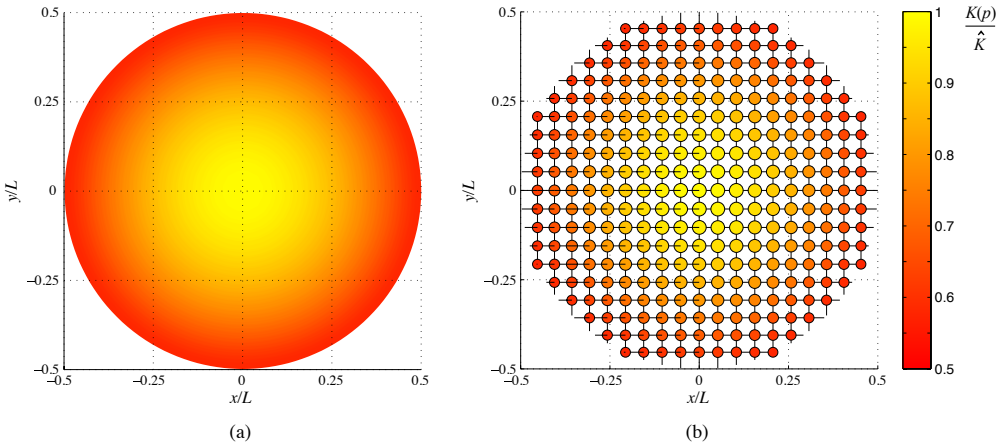

Figure 5: Setup geometry: gaussian curvature of the reference continuous shell surface (a), nodal apex $K(p)$ of the grid shell (b)

behaviour of the SLGS for the specific adopted geometrical and structural setup.

The constitutive model of the steel is linear elastic - perfect plastic, with a yield strength equal to $f_y = 355$ MPa,

Table 1: Mechanical properties of the structural elements

element type (ANSYS©nomenclature)	Area [m^2]	Inertia [m^4]	mass [kg/m]
beam (BEAM188)	$2.5e-3$	$5.2e-7$	19.6
truss (LINK180)	$1.6e-4$	–	1.25

Young's modulus $E = 2.1e+5$ MPa and Poisson's ratio $\nu = 0.3$. The diagonal cable prestressing is equal to $\sigma_0 = 100$ MPa. The dead load g of structural steel members and of 20 mm-thick glass glazing is set equal to 0.5 KN/m^2. As for the live load s, a uniform snow load $s = 0.75$ kN/m^2 is applied on the structure. A symmetrical load case $q = 1.3g + 1.5s$ is applied to the structure. The resultant p-th nodal load is defined as $Q_p = \int_A q da \approx 4000$ N, being A the quadrangle surface.

3.3. Parametric analysis plan

Following the Eigenmode Imperfection Method, the equivalent nodal imperfection field $\boldsymbol{\eta}(p)$ is generally expressed as

$$\boldsymbol{\eta}(p) = \alpha \left[k\boldsymbol{\phi}^{0,i}(p) + (1-k)\,\boldsymbol{\phi}^{0,j}(p) \right], \tag{8}$$

where $\boldsymbol{\phi}^{0,i}(p)$ and $\boldsymbol{\phi}^{0,j}(p)$ are two buckling mode shapes of the perfect structure, k is the weighting factor of the two mode shapes, $\alpha = \alpha^* L$ is the amplitude of the imperfection, and α^* its dimensionless counterpart. The nodal coordinates of the resulting imperfect grid shell are $\mathbf{X}(p) = \mathbf{X}^0(p) + \boldsymbol{\eta}(p)$.
Figure 6-a,b shows the performed computational experiment grid in the $\alpha - i$ (setting $k = 1$) and $\alpha - k$ (setting $i = 1$, $j = 2$) parameter planes, respectively. The investigated values range in the intervals $1e-5 \leq \alpha \leq 3e-1$ m, corresponding to $1/3e-6 \leq \alpha^* \leq 1/100$, $0 \leq i \leq 20$, and $0 \leq k \leq 1$. In other terms, first a single mode shape is adopted as imperfection shape for each of the first 20 buckling modes and for 29 different values of the imperfection amplitude. Second, 2 modes are retained, and 11 convex combinations between them are adopted as imperfection shape for 29 different values of the imperfection amplitude. A total number of 957 imperfect setups is considered. Each setup is analyzed by means of the three structural models described in Section 2.1, i.e. by performing 2871 computational simulations. The stacked histograms of the CPU time are shown in Figure 6-c for each structural model. The mean values of the CPU time required for a single LBA, GNA and GMNA are $\bar{\Delta}t = 3.9, 46.26$ and 48.5 s, respectively. The overall CPU time is equal to about 26h 13' 27".

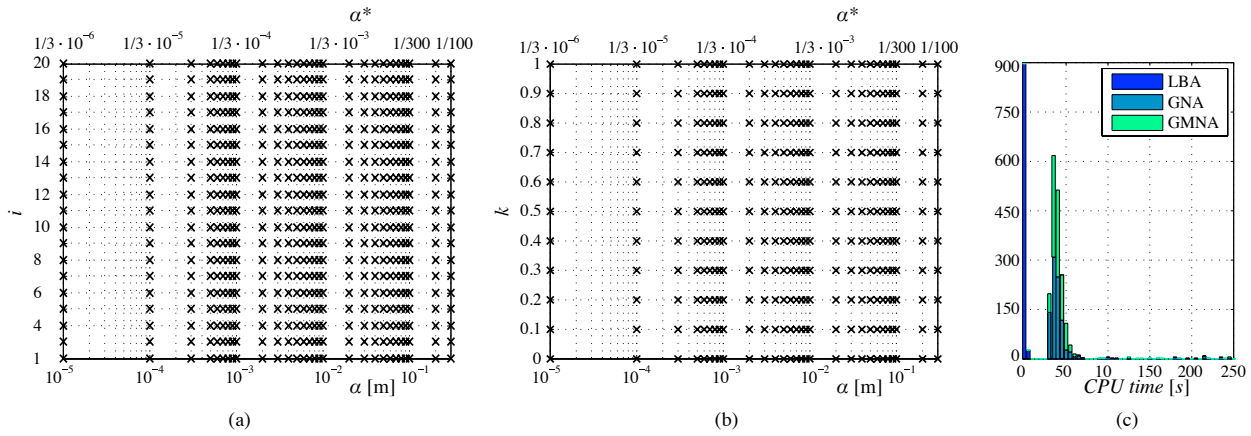

Figure 6: Discretization of the $\alpha - i$ parameter plane (a), $\alpha - k$ parameter plane (b), stacked histograms of the CPU time for a single simulation (c)

4. Application and results

4.1. Perfect setup

The eigenvalues λ (a) and BSL (b) of the first 20 buckling modes of the perfect structure obtained by LBA are collected in Figure 7. The modes are categorized with respect to the main features of their shapes, i.e., by identifying symmetric patterns with respect to the generatrix and directrix or to the diagonals of the quadrants defined by the generatrix and directrix. The first seven modes have eigenvalues very close to each other, while from mode 9 an abrupt increase in the LF value can be observed (Figure 7-a). It is worth pointing out that the modes labelled with red circles appear in couples with the same eigenvalue and mode shapes rotated of 90 degrees. Figure 7-b highlights the presence of both global and local modes. The first two modes show the highest degree of globalness.
A deeper insight into the first three buckling mode shapes is shown in Figure 8. On one hand the first and second mode shapes are clearly global, i.e. the values close to unit are almost uniformly spread along the whole structure (Sect. 2.2). On the other hand, the third mode shape (Fig. 8-c1) has the values close to unit clustered in two limited

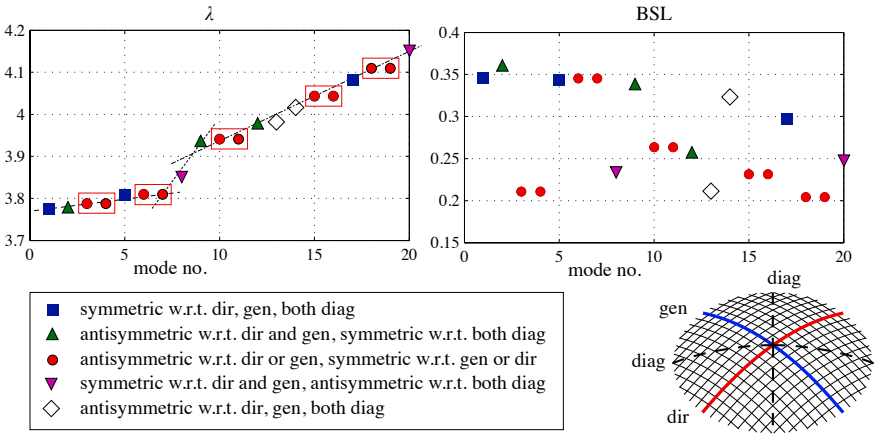

Figure 7: Eigenvalues λ (a) and BSL (b) of the first 20 buckling modes of the perfect structure by LBA

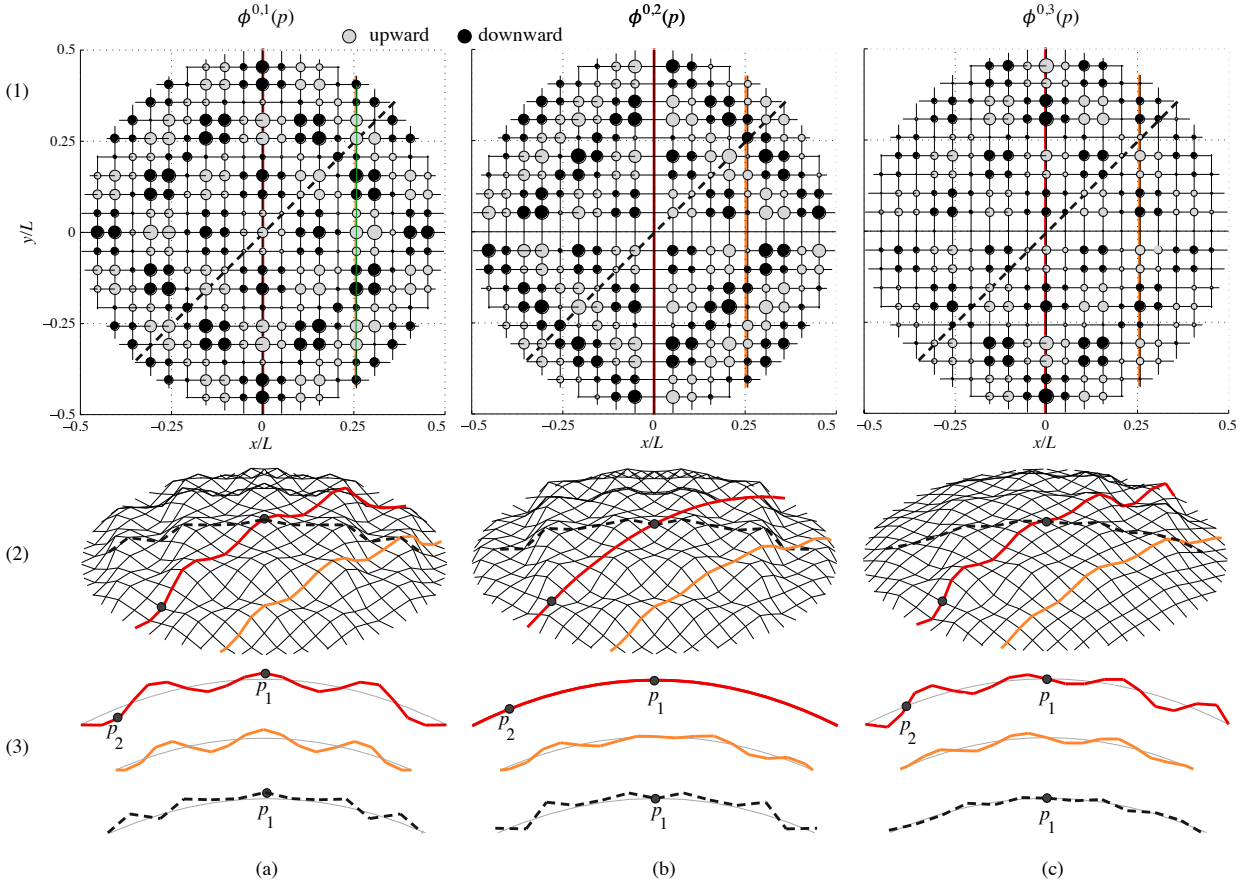

Figure 8: First ($\phi_{1,0}$, a), second ($\phi_{2,0}$, b) and third ($\phi_{3,0}$, c) buckling mode shapes of the perfect structure by LBA

regions. These features agree with the low value of the BSL measure. The first one has a symmetrical mode shape with respect to the directrix and generatrix directions, while the second mode shape is antisymmetric with respect

to both directrix and generatrix, while it is symmetric with respect to the diagonals of the quadrants defined by the directrix and generatrix. The third mode shape is symmetric with respect to the directrix and antisymmetric with respect to the generatrix (or vice versa).

Furthermore, the eigenvalues of the modes have nearly the same value ($\lambda^{0,1} = 3.774$, $\lambda^{0,2} = 3.776$, $\lambda^{0,3} = 3.788$), even though the corresponding mode shapes are quite different. This confirms what already observed in [14]: several buckling modes can occur at nearly the same load level and can nearly equally contribute to the deformed shape at collapse. In other words, a selection criterion based on LF only is not decisive, and at the same time the BSL values provide more information about mode properties, but they do not directly suggest any complementary criteria. Hence, in the perspective of the EIM application, the first mode(s) criterion remains the default one usually adopted in practice. We believe that a correct a-priori choice among modes having almost the same eigenvalue requires additional knowledge and selection criteria.

The load multiplier μ - nodal deflection δ paths of the perfect grid shell obtained by GMNA analysis are plotted in Figure 9-a, for both Load Control (LC-NR) and Arc-Length (AL-NR) path-following procedures. The nodal deflection refers to the node where the displacement is known to be the maximum (red circle in Fig. 9-b). For

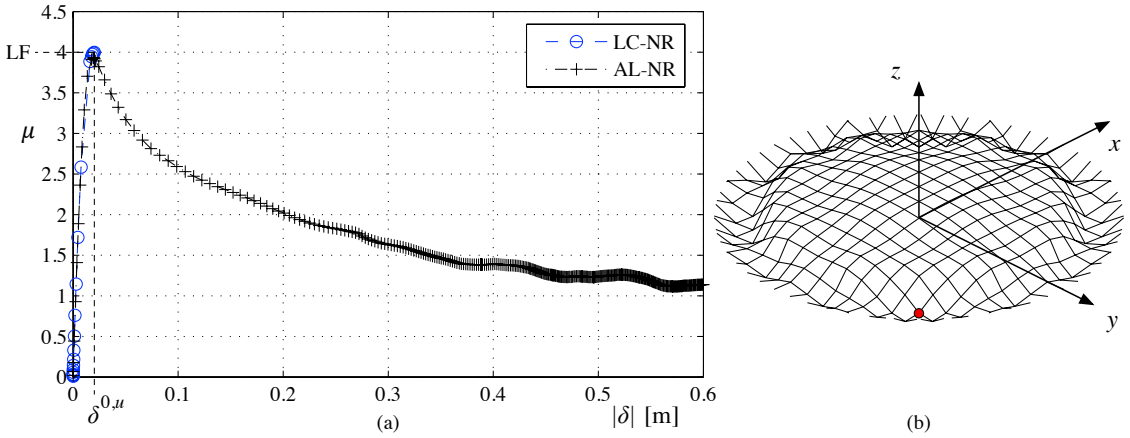

Figure 9: Load multiplier - deflection paths (a) and ultimate deflection field $\delta^u(p)$ (b) of the perfect structure by GMNA

the sake of brevity, the results obtained by GNA are not included, being nearly the same to the ones by GMNA. In other words, plasticity does not take place in the adopted perfect setup, coherently with its slenderness (Section 3). As anticipated, a predominant single mode contribution cannot be recognized in the ultimate deflection field $\delta^u(p)$, (cfr. Fig. 9-b in comparison with Fig. 8). This is expected bearing in mind the very close values of λ for the first modes (Fig. 7-a). While the LC-NR is able to follow the μ - δ up to the critical point u, the AL-NR is able to describe the post critical branch too. Both numerical approaches approximate the same critical limit point. Bearing in mind that the study is focused on the critical condition, that it implies a large number of numerical experiments, and that the AL-NR involves computational costs approximatively 50 time higher than the LC-NR, the latter is retained in the following.

4.2. Imperfect setup: α-i sensitivity analysis

In this section, we first evaluate the dome stability in the parameter plane α-i. The nodal imperfection field results from an imperfection shape equal to the buckling shape of a single mode among the first 20 ones discussed in the previous section, i.e. in formulas $k = 1$, $1 \leq i \leq 20$ (eq 8). For each imperfection shape, the imperfection amplitude ranges in $1e-5 \leq \alpha \leq 3e-1$ m. For the sake of conciseness, only the load factor is examined in this section. For each structural model, it is normalized with reference to the LF of the perfect structure (LF^0). Figure 10 shows the evolution of the normalized LF versus the imperfection amplitude and for each mode shape (grey lines). The envelope of the minima of LF (i.e. the worst case scenario) at each imperfection amplitude is highlighted in red, together with the mode that gives the minimum value (filled markers). It is worth pointing out that:

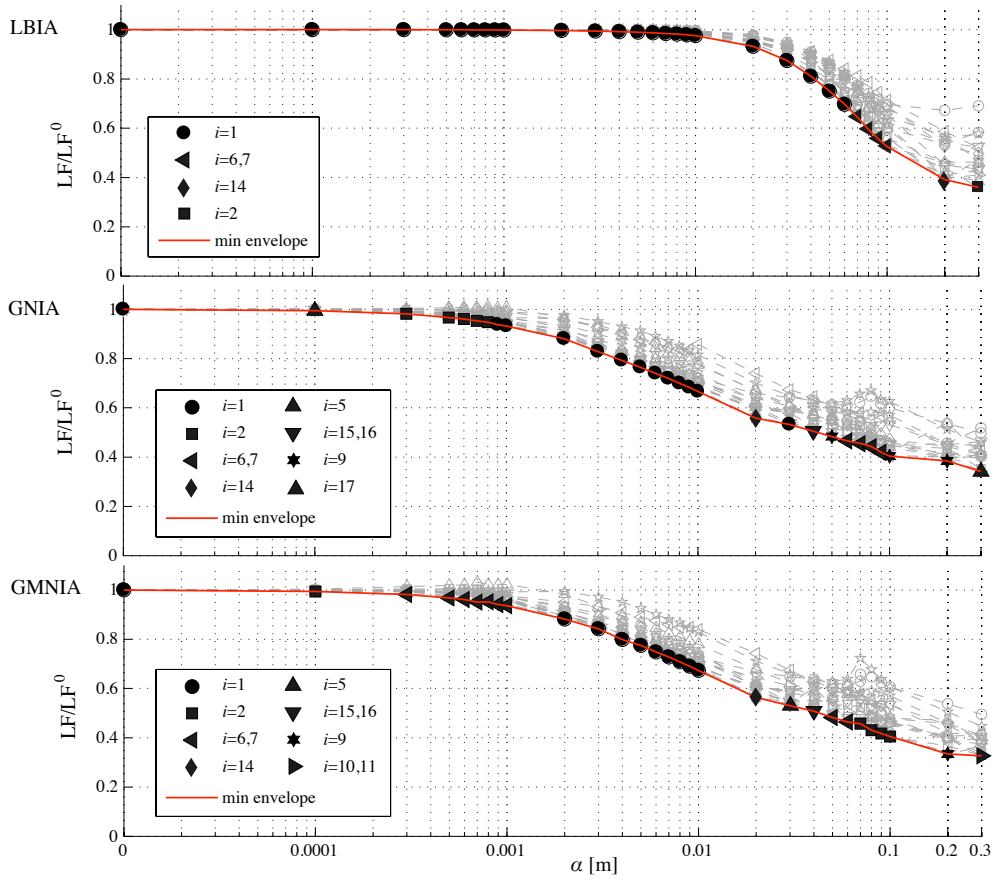

Figure 10: Load Factor versus the nodal imperfection for each modal imperfection shape and for each model: ensemble of the obtained results and envelope of the LF minima

- the higher the imperfection amplitude, the more scattered the LF resulting from different modes. In particular, a significant scatter takes place for $\alpha > 0.01$ m in LBIA, but occurs earlier in GNIA and GMNIA for $\alpha > 0.0001$ m;
- the worst case scenario is given by different mode shapes for varying imperfection amplitude. In particular, the nonlinear models (GNIA, GMNIA) predict a high number of mode shapes (4 in LBIA, 8 in GNIA and GMNIA) and the mode switching occurs for low values of the imperfection amplitude;
- the first mode provides the lowest LF only at very low imperfection amplitude by LBIA, while further ones (e.g. 2 and 5) and high modes (e.g. 10,11,14,15,16) provide the lowest LF by GNIA and GMNIA;
- contribution of mode numbers higher than 20 to the worst case scenario cannot be excluded a priori;
- the modes which contribute to the worst case scenario belong to all the different shapes categorized in Figure 7.
- most of the modes which contribute to the worst case scenario are characterized by high BSL (e.g. 1, 2, 5, 6,7, 9, 14) but some modes antisymmetric w.r.t. directrix or generatrix are not (e.g. 10,11 and 15,16).

In short, a single worst buckling mode to the stability of the structure cannot be identified even for the adopted benchmark, nor a valuable choice criterion can be inferred by the present numerical experiments, although modes having a high degree of globalness (high BSL) seem to prevail. The multiple switches from a worst buckling mode to

another varying the imperfection amplitude is a critical issue in the design perspective. Bearing in mind the features above, the single-mode EIM demonstrates its scarce robustness and predictability of the worst case scenario. The multiple switches, especially at the imperfection amplitudes of design interest ($\alpha^* > 1/500$), are due to the scattered value of the LF obtained by different modes for a given amplitude, and to the occurrence of local maxima in the LF trend versus the imperfection amplitude for a number of modes. In order to shed some more light on this feature, the LF(α) curves are grouped according to the occurrence of local maxima or not. They are plotted in Figure 11 for each structural model. The linear analysis (LBIA) mostly simulates a monotonic trend of LF(α) for all the modes, except

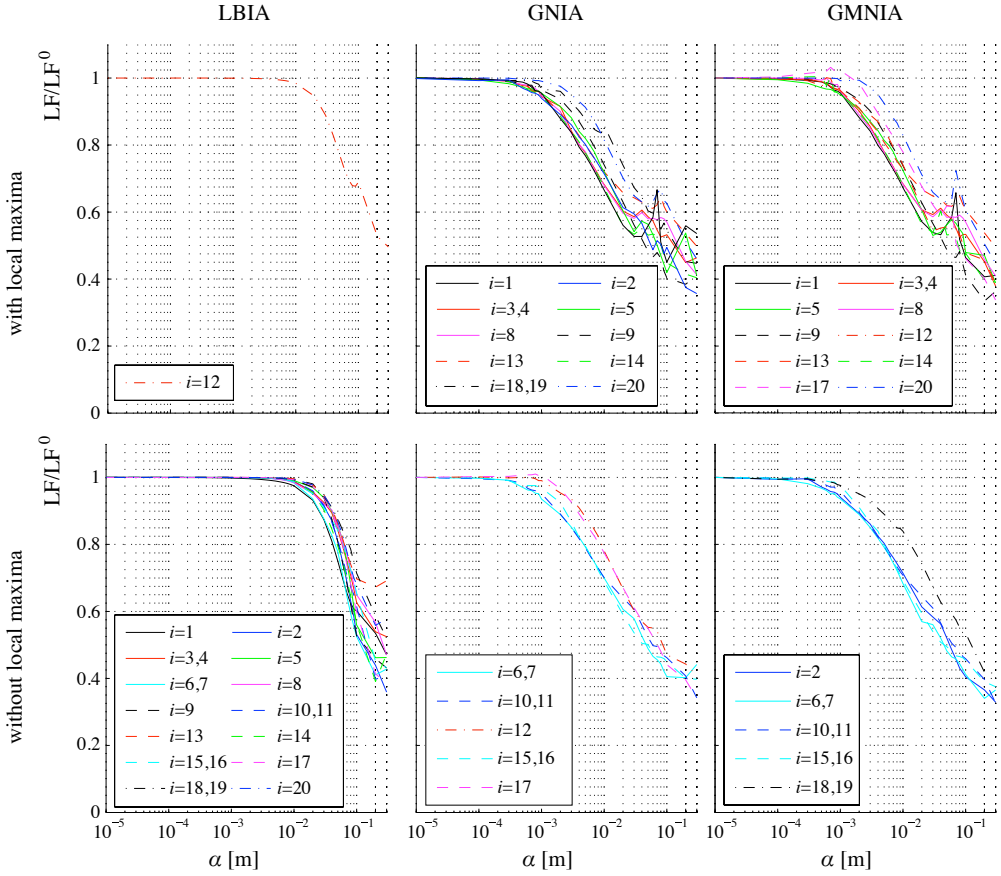

Figure 11: Load Factor versus the imperfection amplitude for each mode shape and structural model: trends with and without local maxima

for one mode (mode 12). Conversely, the more accurate non linear models point out local maxima for the majority of modes at high value of the imperfection amplitude (about $3 \leq \alpha \leq 10$ cm, i.e. $1/1000 \leq \alpha^* \leq 1/300$). Generally speaking, GNIA and GMNIA provide analogous results from a qualitative point of view. In other terms, the effects of the geometric non linearity largely prevail on the mechanical ones for the adopted benchmark, as expected. However, some differences occur at high values of α, e.g. $\alpha \geq 7$ cm, i.e. where local maxima take place. These differences induce some modes to move from one group to another. In particular, mode 1 give rise to two high peaks in LF by GNIA, and a single one in GMNIA. Analogously, mode 2 involves two weak peaks in GNIA, but the same mode shows a monotonic trend in GMNIA. Such differences are due to localized plastic behavior of structural members, which reduce the limit load, properly simulated by GMNIA. In short, it is worth pointing out that local maxima: i. mostly occur at relatively high values of the imperfection amplitude of interest for designers; ii. affect both low mode numbers, notably mode 1, and high ones, e.g. node 20. In other terms, the rule "the higher the imperfection amplitude, the lower the load factor" is mostly unfulfilled. The designer is in the uncomfortable position of having to deal both with the choice of the single mode to be adopted as imperfection shape and of the imperfection amplitude. Both seem

uncertain and strongly affect the load factor.

4.3. Imperfect setup: α-k sensitivity analysis

Having in mind the results obtained for single-mode imperfection shapes, we aim at further assess the dome stability by adopting a combination of two modes. Mode 1 and mode 2 involve a monotonic trend of $LF(\alpha)$ in LBIA, and one or more local maxima of $LF(\alpha)$ in GNIA. Furthermore, in GMNIA mode 1 causes a local maximum of $LF(\alpha)$, while mode 2 causes a monotonic trend of $LF(\alpha)$. Hence, we cover a wide casuistry by selecting mode 1 and mode 2, or in formulas $i = 1$, $j = 2$ (eq 8). The LF and BSL are evaluated for each imperfect setup in the $\alpha - k$ plane, and for each structural model. They are plotted in Figure 12 for the sake of completeness and brevity. In order to allow a

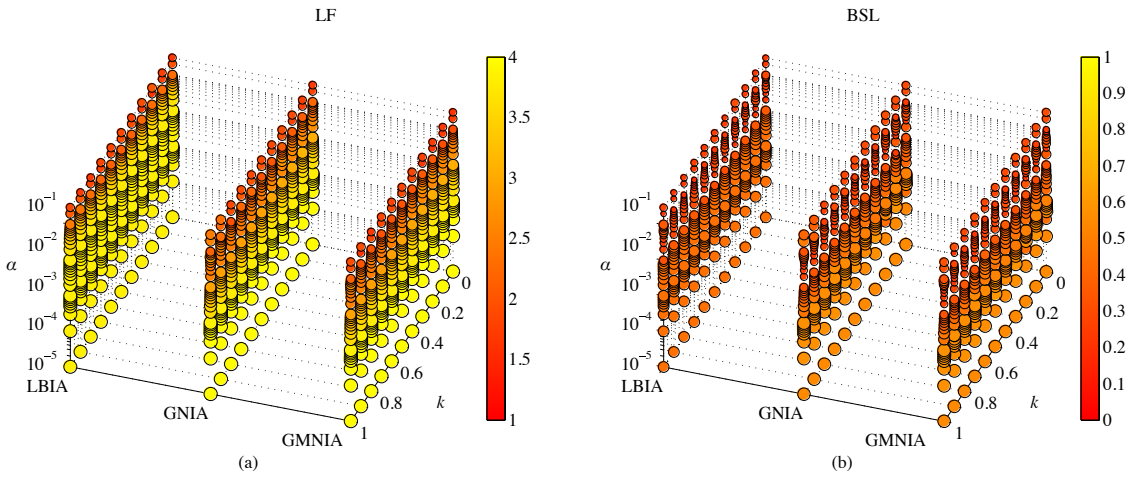

Figure 12: Synopsis of the bulk parameters versus the nodal imperfection and the structural models

more detailed reading, the trend of the bulk quantities versus the imperfection is separately plotted for each model in Figure 13. Moreover, the trend of the bulk parameters versus α is plotted for each structural model in Figure 14 at the extreme values of the weighting factor $k = 1$ and $k = 0$, corresponding to the imperfection field equal to the first and second buckling mode, respectively.

The load factor LF resulting from LBIA is nearly insensitive to the imperfection shape, i.e. for constant α and varying k. An analogous overall trend holds for BSL, even if it is no longer fully monotonic versus α and not exactly constant versus k for $\alpha \geq 1$ cm. Conversely, the non linear analyses GNIA and GMNIA reveal a higher sensitivity of both the bulk parameters to the imperfection shape. The BSL value of the perfect grid shell predicted by GNIA/GMNIA (BSL ≈ 0.47) is higher than the one predicted by LBIA (BSL ≈ 0.35), that is, a higher degree of globalness at collapse results from the geometric non linearity. The growth of the imperfection amplitude α significantly reduces the globalness to BSL ≈ 0.1 In other terms, the imperfection generally induces a localization of the collapse.

In Figure 13 the local maxima of LF are highlighted by circular blue markers. Local maxima are significantly scattered within the whole k range and for $\alpha \geq 0.3$ by both the nonlinear models.. In particular, in the GMNIA model, the local maximum for $k = 1$ (mode 1) intermittently occurs also for $k = 0.9, 0.8, 0.3, 0.2, 0.1$, while a monotonic trend is observed for the remaining values of k, including mode 2 (k=0). In other terms, even though mode 1 ($k = 1$) and mode 2 ($k = 0$) cause different trends of LF(α), decreasing k does not progressively smooth the peak from mode 1 to mode 2. Once more, the designer who applies a two-mode imperfection shape within EIM approach is in the uncomfortable position of having to deal with a further choice about the value of k, beside the selection of the modes i, j and the imperfection amplitude α.

In summary of Sections 4.2 and 4.3, no general criteria can be drawn from the numerical experiments and for the adopted setup to properly choose the buckling mode shape(s) i, the value of the imperfection amplitude α, and to get the weighting factor k. These difficulties are expected to be even greater for more complex structural forms.

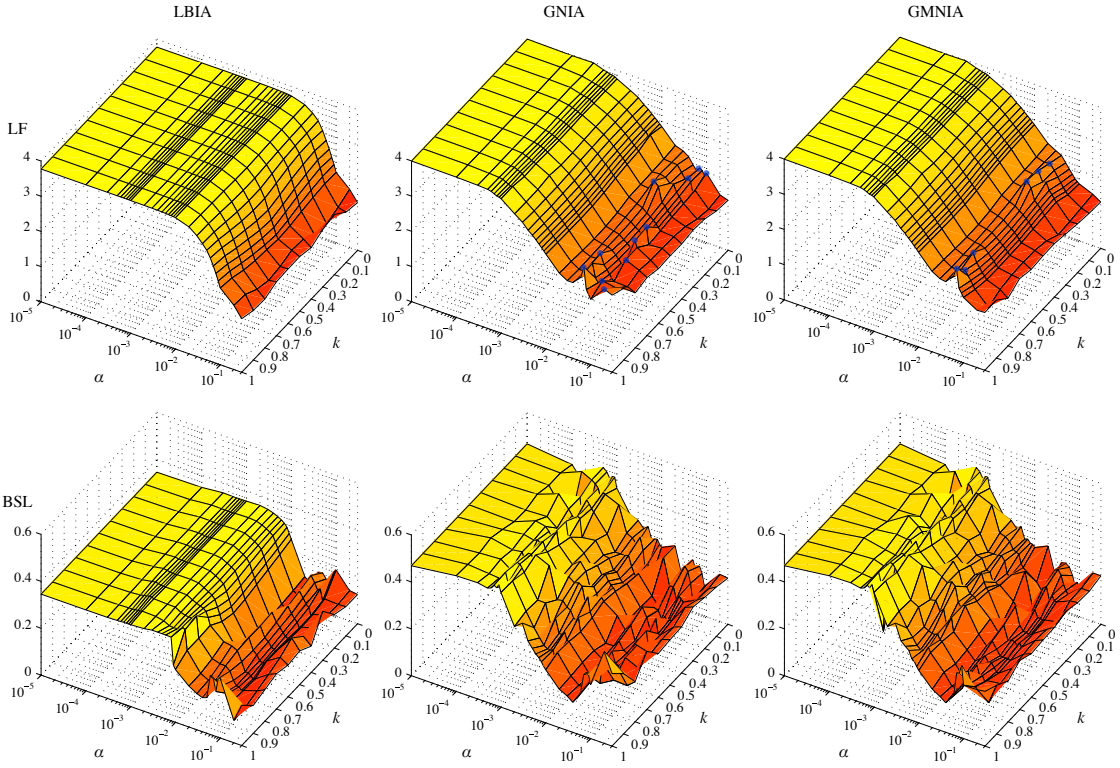

Figure 13: Trend of the bulk parameters versus the nodal imperfection for the three structural models

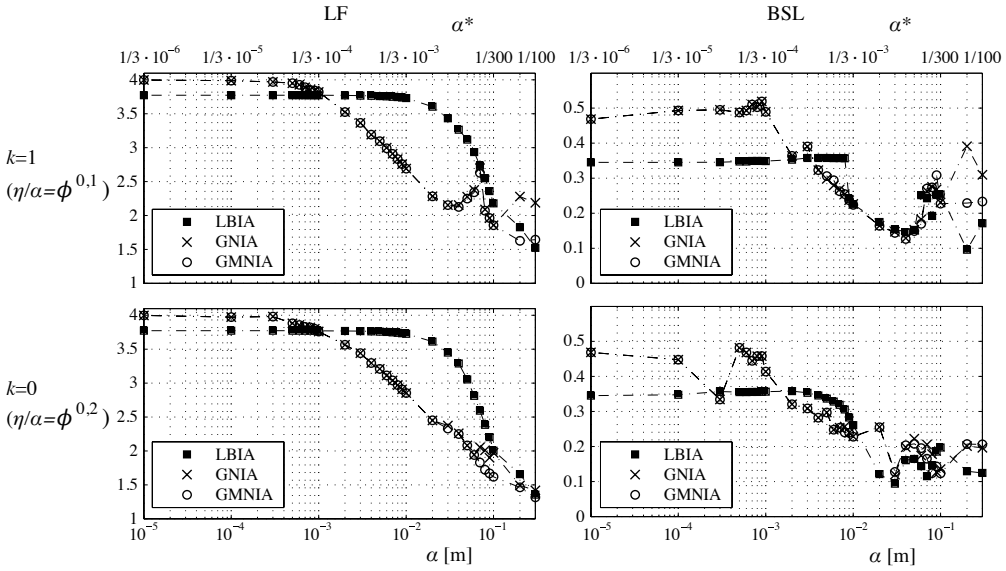

Figure 14: Trend of the bulk parameters versus the imperfection amplitude for the three structural models. Imperfection patterns coincident to the 1st ($k = 1$) and 2nd ($k = 0$) mode shape

4.4. *Imperfect setup: mechanical reading*

This section aims at providing a deeper insight in the ultimate mechanical behaviour of the grid shell for varying α in order to point out the causes of the high sensitivity to the imperfection highlighted in the previous Section. In the following the most detailed mechanical model is retained (GMNIA) and the weighting factor is set equal to $k = 1$ ($\eta/\alpha = \phi^{1,0}$).

To investigate the existence of a relationship between LF and BSL, the former is plotted against the latter in Figure 15. Both parameters are scaled with respect to their values obtained for the perfect setup (LF^0 and BSL^0). In spite

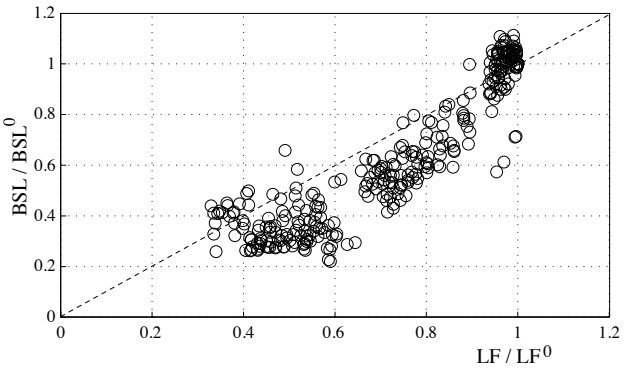

Figure 15: GMNIA model: LF versus BSL

of a certain dispersion of data, a clear trend can be recognised: the higher the LF, the higher the BSL, and vice versa. This result can be interpreted as a general trend towards high degree of localness of the deformed shape at collapse for decreasing value of the LF.

4.4.1. *Regime identification*

The evolution of the main bulk parameters versus the imperfection amplitude α is plotted in Figure 16. Homogeneous

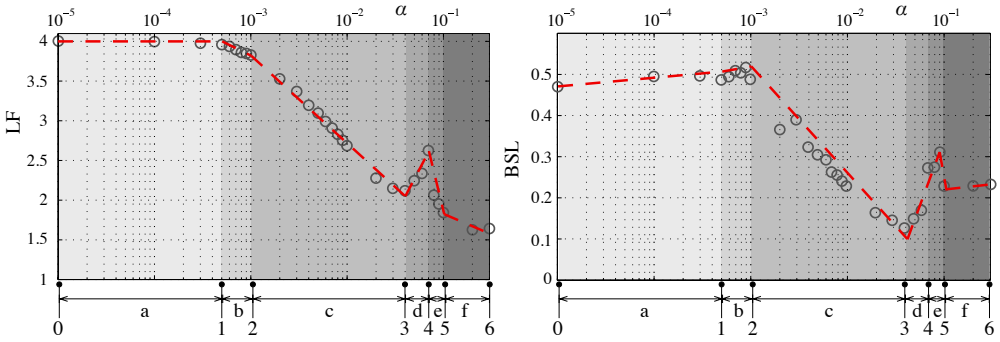

Figure 16: Recognized regimes for $k = 1$

intervals of α are recognized with respect to the trend of the LF. It is worth pointing out that BSL shows coherent trends. The α intervals and the corresponding boundary values are labelled by latin letters and numbers, respectively. Five ranges are selected. Regime "a" corresponds to very low values of the imperfection magnitude ($1e-5 \leq \alpha \leq 5e-4$) and its lower bound "0" can be confused with the perfect geometry: in this range, the imperfection does not have effects on LF and does not significantly impact on BSL. The regime "b" ($5e-4 \leq \alpha \leq 1e-3$) is a transition one where the slight descent of LF corresponds to an analogous growth of BSL. The regime "c" ($1e-3 \leq \alpha \leq 4e-2$) shows the significant exponential decrease of both LF and BSL. The watershed "4" between

regimes “d” and “e” is defined at the local maximum of both LS and BSL. Finally, the “f” regime corresponds to a smooth decrease of the LF and a corresponding constant trend of BSL. It is worth pointing out that the watershed values between two successive regimes, and the existence of regimes “d” and “e”, depend on the value of the weighting factor k for the selected benchmark (see Figure 13), and they are expected to vary with the geometrical and mechanical parameters of the grid shell.

The load multiplier μ - nodal deflection δ paths obtained by GMNIA analysis at the recognized regime bounds are plotted in Figure 17-a. The nodal deflection refers to the node where the displacement is known to be the maximum at each bound. The setups corresponding to the regime bounds show different initial stiffness (Figure 17-b), generally

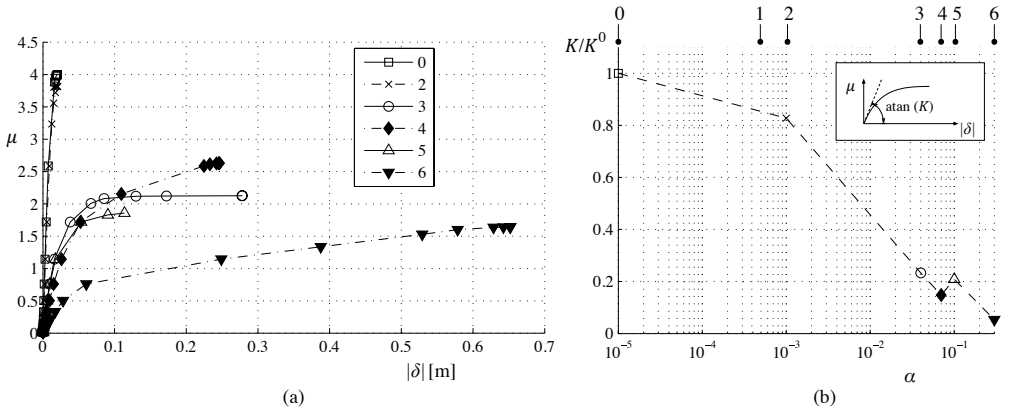

Figure 17: Load - deflection paths by GMNIA and $k = 1$ for the recognized regime bounds (a) and corresponding initial stiffness k (b)

decreasing with the increase of the imperfection, except in the range between regime bounds 4 and 5, where a small growth appears. The same occurs for the non linear evolution of the deflection: the ultimate displacement before collapse is dramatically increased by the presence of imperfections, except in case of regime bound 5. The perfect setup is highly stiff, due to its parabolic shape, but collapse is more sudden than in the imperfect ones.

4.4.2. Correlation between the imperfection pattern and the deformed shape at collapse

Figure 18 represents the spatial distribution of the “input” imperfection and the resulting spatial distribution of the mechanical “output” for each one of the identified regime transitions. The imperfection is expressed by both the component of the nodal imperfection $\eta_v(p)$ evaluated along the direction v, and by the nodal apex K, calculated for the imperfect geometry. Correspondingly, the collapse shape is expressed by both the component of the nodal displacement $\delta_v^u(p)$ evaluated along the direction v, and by the nodal apex $K^u(p)$. The figure aims at highlighting the imperfection and ultimate deflection patterns, therefore all quantities are normalized to their maximum value. Hence, the field $\eta_v/\hat{\eta}_v$ is common to every regime transitions.

The following remarks can be outlined:

- a qualitative visual comparison between the nodal imperfection and ultimate displacement patterns reveals poor correlation between them;
- the pattern of the nodal displacement at collapse $\delta_v^u(p)$ strongly varies across the regimes. In general, the higher the magnitude of the imperfection, the more localized the displacement and the lower the degree of globalness (BSL, Fig. 16), with the exception of bound 4, where a local maximum of the BSL has been detected. In particular, at bound 3 the displacement field is localised in four regions in the neighbourhood of node p_2 and its counterparts along the directrix and the generatrix;
- the pattern of the nodal apex $K(p)$ varies across the regimes, and a high correlation can be qualitatively recognized with the nodal displacement at collapse $\delta_v^u(p)$. The closer to zero the nodal apex of the imperfect shell, the higher its nodal displacement at collapse;

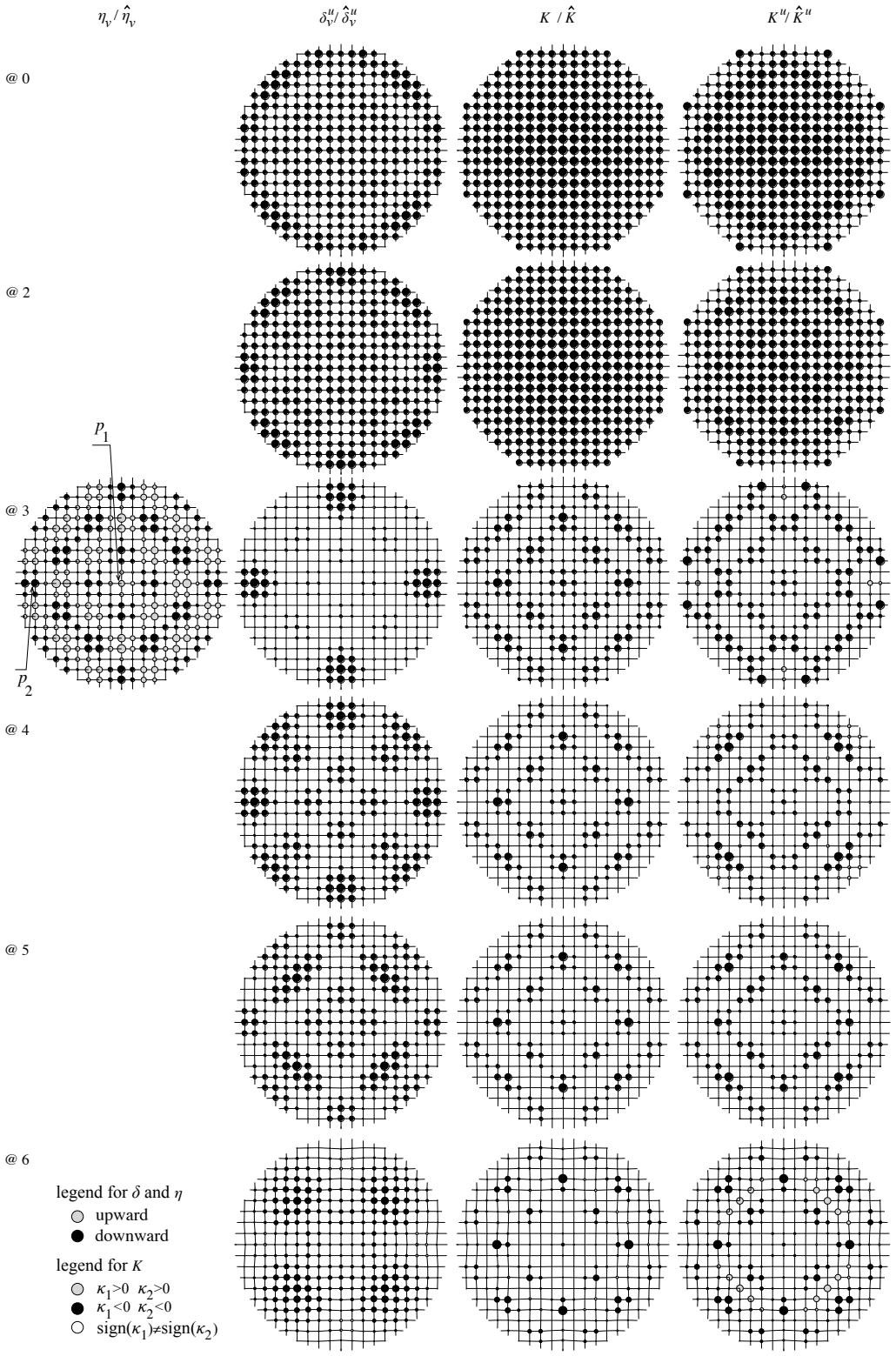

Figure 18: Regime transitions: imperfection, displacements at collapse, nodal apex of the imperfect geometry, and nodal apex of the collapse shape

- the patterns of the nodal apex $K(p)$ and the one of nodal apex at collapse $K^u(p)$ show the highest correspondence. This means that the deformation at collapse maintains and slightly modifies the apex of the initial imperfect geometry.

In order to check in a synthetic and quantitative way the correlation heuristically pointed out above, let us introduce the correlation coefficient $R(i, j)$ $[-1 : 1]$ classically defined as

$$R(i, j) = \frac{cov(i, j)}{\tilde{i}\ \tilde{j}} = \frac{E\left[\left(i - \bar{i}\right)\left(j - \bar{j}\right)\right]}{\tilde{i}\ \tilde{j}} \tag{9}$$

where $i(p)$ and $j(p)$ refer to the fields to be compared, $\tilde{i}$ is the standard deviation, $\bar{i}$ is the mean value, E is the expected value operator, cov is the covariance. In particular, the correlation coefficient is adopted in order to check the correlation of the input imperfection field with the output ultimate deflection. Hence $i = \eta_v(p)$ and $j = \delta_v^u(p)$, or $i = K(p)$ and $j = K^u(p)$. The correlation coefficients defined above are plotted versus k and α in Figure 19. The obtained results

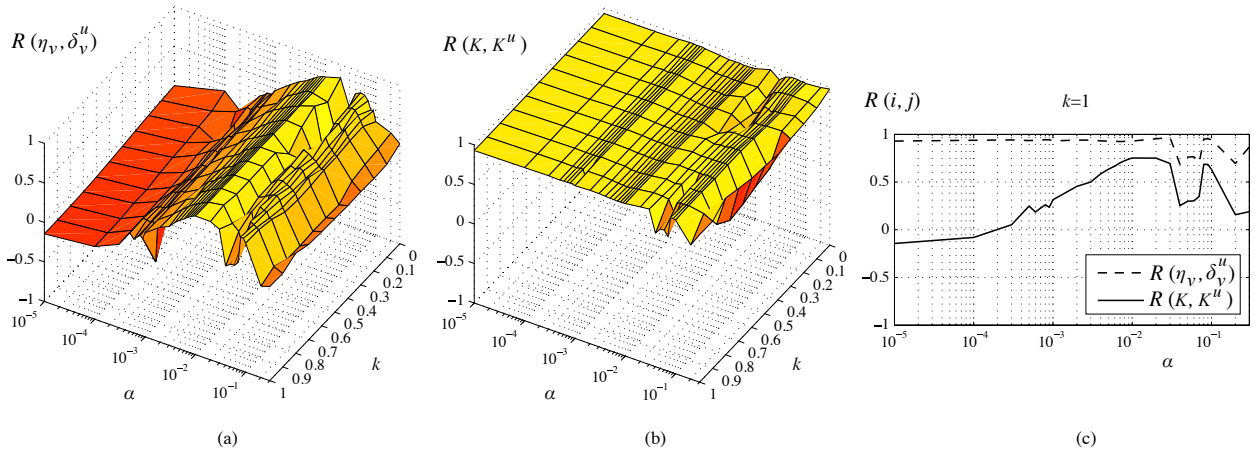

Figure 19: Correlation coefficient $R(i, j)$ for the analysed pairs of metrics of input imperfection and output deflection at collapse as a function of α and k (a,b) and for $k = 1$ (c)

clearly and quantitatively testify that a low correlation exists between the input-output pair $\eta_v - \delta_v^u$, while the $K - K^u$ pair is highly correlated. The diminished correlation at about $0.04 < \alpha < 0.07$ is due to the significant geometric non linear effects taking place because of the large displacements at collapse.

Beside the above correlation, in the following some light is shed on the mechanical role played by the apex. Generally speaking, when the apex in a node vanishes, the grid shell locally approaches a flat grid and its geometrical stiffness tends to zero. Such a trend reflects the well-known shape-resistant behaviour of domes. In particular, the apex of the imperfect shape depends both on the perfect shape and on the applied imperfection. Its upward or downward direction induces the local increase or the decrease of the perfect apex, respectively. In order to give evidence to these issues, the evolution of K, K^u and δ_v^u versus the imperfection amplitude α is plotted in Figure 20 for the nodes p_1 and p_2 (Fig. 3). In p_1 (Fig. 20-a) the nodal apex of the perfect structure has the maximum value (Fig. 5-b) and the nodal imperfection is upward according to the shape of the first mode (Fig. 8-a). Hence the imperfection increases the nodal apex and the local geometrical stiffness of the shell in turn, resulting in a "imperfection stiffening". Conversely, in p_2 (Fig. 20-b) the nodal imperfection is downward according to the shape of the first mode. Hence the imperfection reduces the nodal apex and the local geometrical stiffness of the shell in turn, resulting in a "imperfection softening". In this second case, if the nodal apices of the perfect geometry and of the imperfection are opposite, the apex of the imperfect geometry tends to zero and so the local stiffness. From Fig. 20-b a significant growth of the displacement takes place at $\alpha_A = 0.02 \leq \alpha \leq \alpha_B = 0.03$, before the nodal apex $K(p_2)$ reaches zero ($\alpha_C = 0.07$). Such shift effect can be explained as follows. At both α_A and α_B the nodal apex K changes significantly at collapse: in the first case it becomes negative ($sign(\kappa_1) \neq sign(\kappa_2)$), in the second the shell convexity is oriented downward ($\kappa_1 < 0, \kappa_2 < 0$). In

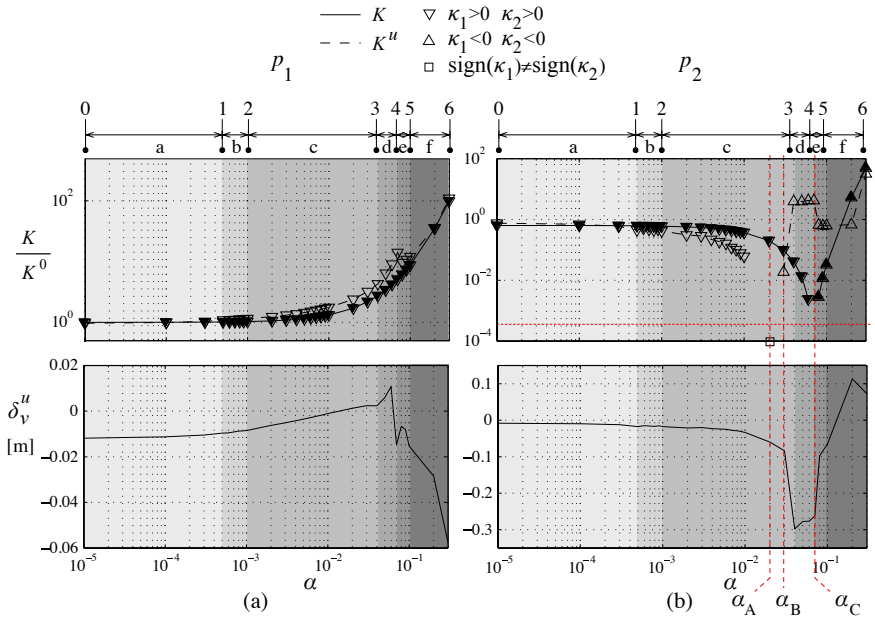

Figure 20: Sensitivity of the initial and ultimate nodal apex, and of the ultimate displacement to the imperfection magnitude for the nodes p_1 and p_2 (see Fig. 3)

such situations, a small but not zero nodal apex K on the imperfect shell involves $K^u = 0$ at collapse.

5. Conclusions

The present study is addressed to contribute to the deep understanding of the effects of the Equivalent Geometric Nodal Imperfections on the buckling instability of a hybrid single layer grid shell by means of the Eigenmode Imperfection Method. A given SLGS dome is adopted as a benchmark. The imperfection shape is obtained by adopting single modeshape among the first 20 ones and by weighting the shapes of two modes. The range of the weighting factor and of the imperfection amplitude is densely resolved compared to the previous studies available in literature.

The EIM has been critically reviewed on the basis of the results of numerical experiments. The main findings are summarized in the following:

- the growth of the imperfection amplitude does not necessarily involve the decrease of the Load Factor: in fact, local maxima of LF take place along a general decreasing trend versus α. Hence, assuming high imperfection amplitude is not an a priori conservative choice that involves the worst case scenario;
- a single worst buckling mode to the stability of the structure cannot be identified, because different modal imperfection shapes contribute to the worst case scenario at different values of the imperfection amplitude;
- imperfection shapes resulting from the combination of two mode shapes additionally suffer the uncertainty about the weighting coefficient.

In short, the EIM does not seem to be grounded on general phenomenological bases and its extension to the ultimate buckling state is questionable even for the relatively simple grid shell scrutinized in this study. Generally speaking, the EIM is affected by epistemic uncertainties about its main parameters (imperfection shape and amplitude) which severely affect its predictability. The huge variety of grid shell typologies and of structural shapes it is expected to make even more questionable the extension of the results to a wider domain of application. For the time being, special

care should be paid for EIM application in the design practice. More general and more robust models of the Equivalent Geometric Nodal Imperfection in a worst case scenario perspective are needed in the near future.

Bearing such a need in mind, we have intended to contribute to the understanding of the buckling instability of the adopted benchmark. The main findings are summarized in the following:

- a new observable, called Buckling Shape Length, has been introduced to quantify the degree of globalness of the deformed shape at collapse. The BSL appears to be somewhat related with the Load Factor. A general trend has been identified, where lower values of the LF correspond to decreasing values of the BSL: in other words, the reduction of the ultimate carrying capacity of the structure - generally related to increasing imperfection amplitudes - corresponds to the occurrence of more local deformed shapes at collapse;

- a new metric, called nodal apex, has been identified as the local geometrical parameter that mainly drives the buckling of the studied single layer grid shell. This result suggests to define and set the nodal imperfection in terms of such a metric rather than in terms of the deviation from the perfect geometry along the direction normal to the reference surface.

We hope that making reference to these metrics could allow to phenomenologically ground future models of the Equivalent Geometric Nodal Imperfection able to predict the worst case scenario.

Acknowledgements

The authors wish to thank Claudio Canuto, Department of Mathematical Sciences at Politecnico di Torino, for the fruitful discussions about the topics of the paper.

References

[1] V. Gioncu, Buckling of reticulated shells: State-of-the-art, International Journal of Space Structures 10 (1) (1995) 1–46.
[2] JGJ61-2003 Technical specification for reticulated shells. Beijing: China Architecture Industry Press, 2003 [in Chinese].
[3] EN 1993-1-6:2007 Eurocode 3: Design of steel structures - Part 1-6: Strength and stability of shell structures. European Committee for Standardization, 2007.
[4] C. de Paor, K. Cronin, J. Gleeson, D. Kelliher, Statistical characterisation and modelling of random geometric imperfections in cylindrical shells, Thin-Walled Structures 58 (2012) 9–17.
[5] R. Peek, Worst shapes of imperfections for space trusses with multiple global and local buckling modes, International Journal of Solids and Structures 30 (16) (1993) 2243–2260.
[6] C. Borri, P. Spinelli, Buckling and post-buckling behaviour of reticulated shells affected by random imperfections, Computer & Structures 30 (4) (1988) 937–943.
[7] J. Cai, L. Gu, Y. Xu, J. Feng, J. Zhang, Nonlinear stability analysis of hybrid grid shells, International Journal of Structural Stability and Dynamics 13 (1) (2013) 1–16.
[8] F. Fan, Z. Cao, S. Shen, Elasto-plastic stability of single-layer reticulated shells, Thin-Walled Structures 48 (2010) 827–836.
[9] J. Sischka, Widespan roof structures, Thomas Telford, London, 2000, Ch. Engineering the construction of the Great Court roof for the British Museum, pp. 199–207.
[10] M. Schlaich, U. Burkhardt, L. Irisarri, J. Goni, Palacio de comunicaciones - a single layer glass grid shell over the court of the future town hall of Madrid, in: Proceedings IASS Symposium 2009, Evolution and trends in design, analysis and construction of shell and spatial structures, International Association for Shell and Spatial Structures, 2009, pp. 1338–1348.
[11] S. Yamada, A. Takeuchi, Y. Tada, K. Tsutsumi, Imperfection-sensitive overall buckling of single-layer lattice domes, Journal of Engineering Mechanics 127 (2001) 382386.
[12] A. Zhang, X. Zhang, J. Ge, Influence of initial geometrical imperfections on stability of a suspendome for badminton arena for 2008 olympic games, Spatial Structures 12 (4) (2006) 8–12 [in Chinese].
[13] J. Guo, Research on distribution and magnitude of initial geometrical imperfection affecting stability of suspendome, Advanced Steel Construction 7 (4) (2011) 344–358.
[14] T. Bulenda, J. Knippers, Stability of grid shells, Computer & Structures 79 (2001) 1161–1174.
[15] S. Yamada, Buckling load evaluation method for single layer cylindrical lattice shells, Journal of Civil Engineering and Architecture 6 (3) (2012) 268279.
[16] S. Malek, T. Wierzbicki, J. Ochsendorf, Buckling of spherical cap grid shells: A numerical and analytical study revisiting the concept of the equivalent continuum, Engineering Structures 75 (15) (2014) 288–298.
[17] S. McCormick, C. Besjak, D. S. Korista, W. Baker, Shell of steel, Civil Engineering - ASCE 73 (4) (2003) 68–73.
[18] J. Cai, Y. Xu, J. Feng, J. Zhang, Nonlinear stability of a single-layer hybrid grid shell, Journal of Civil Engineering and Management 18 (5) (2012) 752–760.

[19] J. Schlaich, H. Schober, Glass-covered grid-shells, Structural Engineering International 6 (2) (1996) 88–90.
[20] SAS IP, Inc., ANSYS, Inc. Theory Manual. (2011).
[21] F. Fan, J. Yan, Z. Cao, Elasto-plastic stability of single-layer reticulated domes with initial curvature of members, Thin-Walled Structures 60 (2012) 239–246.
[22] J. Glymph, D. Shelden, C. Ceccato, J. Mussel, H. Schober, A parametric strategy for free-form glass structures using quadrilateral planar facets, Automation in Construction 13 (2) (2004) 187–202.
[23] A. López, I. Puente, M.A. Serna Direct evaluation of the buckling loads of semi-rigidly jointed single-layer latticed domes under symmetric loading, Engineering Structures 29 (2007) 101–109.